# Trajectory analysis of circulating tumor cells through contorted deterministic lateral displacement array for unruptured trapping: a simulation study

**Rituraj Bhattacharjee[1]** · **R. Kumar[2]**

## Abstract

During the multistage process of cancer spread, fragments of cells branch out from the primitive tumor tissue and scatter throughout the body by blood flow stream or lymph, which are termed as circulating tumor cells (CTCs), regarded as an important biomarker for early cancer diagnosis. Deterministic lateral displacement (DLD) is one of the most efficient passive type particle isolation techniques which functions on asymmetrical laminar flow diversion around the placed microposts forming an array, based on the critical dimeter of the device. In this simulation study, complete trajectory analysis of CTCs and WBCs has been performed using COMSOL Multiphysics software with respect to the angular orientation of sample inlet channel. A simulated model of an asymmetric DLD array-based microfluidic device with latest empirical expression for critical diameter has been presented with optimized sample inlet orientation so as to maintain perfect separation efficiency of CTCs along with arrangement for unruptured trapping of CTCs and WBCs. The approximate CTC isolation efficiency was obtained above 95% for sample inlet inclinations up to 0.5°, and further tilt showed reduction in efficiency. Migration angle of CTC trajectory for the modeled device was obtained around 15° for both the sample inlet orientations leading to least intermingling of CTCs and WBCs. A smaller number of CTC–WBC interaction points was observed for clockwise sample inlet tilt compared to the anticlockwise displacement reducing possibilities of cell rupture. The shear rate around central microposts was found to be higher as well in clockwise sample inlet orientation. This simulation study establishes that sample inlet clockwise tilting of maximum around 0.5°–0.7° leads to better CTC isolation and provides better chances of unruptured trapping of cells at the designated outlets. The results of this study provide an approach toward further optimization of DLD devices' functioning and, thus, could help fabricate better DLD-based microfluidic devices for efficient trapping of CTCs.

**Keywords** Circulating tumor cells · Cancer · Deterministic lateral displacement · DLD · Microfluidics · COMSOL multiphysics · Bio-particles · Cell separation

# 1 Introduction

Cancer, which is a potential killer disease relates to the uncontrolled process of division of mutant cells which goes on till the previous cancer-causing cell, finally duplicates to a lump of cells referred to as tumors. The dangerous health hazard caused by tumors is their invasion of healthy tissues and spread across the body. This process with multiple stages in which cancer is spread within the body of patients involving several organs is termed as cancer metastasis. In the meantime, fragments of cells from the primitive tumor tissue scatter across the body by blood flow stream or lymph, which are referred to as circulating tumor cells (CTCs) [1]. However, observation and analysis of CTCs in the primitive stages when metastasis is showing progression are of vital

Technical Editor: Daniel Onofre de Almeida Cruz.

✉ Rituraj Bhattacharjee
  rituraj.b@manipal.edu

  R. Kumar
  rajagopal.kumar4@gmail.com

[1] Department of Instrumentation and Control Engineering, Manipal Institute of Technology, Manipal Academy of Higher Education, Manipal, Karnataka 576104, India

[2] Department of Electronics and Instrumentation Engineering, National Institute of Technology Nagaland, Dimapur, Nagaland 797103, India

importance for the study of cancerous cells [2]. With a noble intention of early detection of cancerous growth in suspected patients, diverse researchers have converged their attention toward CTC trapping from blood as a fluid biopsy targeted at early identification and treatment of cancer. Proper genetic study about CTCs and experimentation on the treatment efficiency of suitable drugs deliver promising information to help eliminate these cells and prevent spread of cancer [3]. Tracking and identifying such cells in the human blood circulation system pose a challenge since they appear in scarce numbers than other blood cells. For an instance, one milliliter of human blood of an adult contains on an average close to 5 billion red blood cells (RBCs) and between 4000 and 11,000 white blood cells (WBCs) whereas only 10–15 CTCs are found for the same quantity of blood from cancer patients at the progressive metastasis stage [4]. However, an important identifier for CTCs is that they show contrasting physical and biochemical properties compared to blood cells [5, 6]. Most of the CTCs are bigger in size and possess different surface proteins in comparison with RBCs and WBCs. Blood platelets, RBCs and WBCs range within 5 and 15 μm in diameter, and on the other hand, the average size of CTCs range within 15 and 25 μm [7]. Most of the methods devised for targeted isolation of CTCs are based on label-free isolation, including microfluidic filters [8, 9], inertial focusing [10], deterministic lateral displacement (DLD) [11], acoustics [12] and dielectrophoresis (DEP) [13]. The fundamental basis of operation of these methods is that CTCs are bigger in size and exhibit more stiffness than regular blood cells. As a matter of fact, these passive and active methods exhibit their limitations. Acoustics-based method and DEP need additional force fields to operate and take a lot of process time whereas inertial focusing-based approach and microfluidic filter designs suffer from clogging issues.

In the recent age of miniaturization, various researchers are employing microfluidics-based devices owing to their wide range of advantageous features compared to traditional methods [14]. Requirement of minimum volumetric quantity of sample, huge surface-to-volume ratio, fast rate of processing and higher throughput capability are some of the striking features provided by BioMEMS-based devices [15, 16]. These devices have found huge acceptance these days in biomedical fields like drug delivery [17] and cell isolation [18]. Distinguishing by means of separating particles is a very useful approach in different cell-related studies and biochemistry fields. Specifically, separating cells based on certain parameters is of extreme importance in the modern therapeutic studies, cell biology and diagnostics [19]. There can be two approaches of separating bio-particles such as cells—active and passive. In active approach, some kind of an external power source is employed which can be electrical, magnetic or acoustic. On the other hand, passive approach-based methods rely on the microfluidic device

geometry, orientation of flow patterns and its interaction with internal geometrical arrangement [20]. Simpler design, miniature device layout and affordable construction costs are some vital features which make passive devices more popular. Many passive methods of cell separation, thus, have been studied and analyzed recently [21].

DLD is undoubtedly a promising passive method that segregates floating particles based on their structural sizes. With the primitive introduction of DLD back in 2004 [22], this method has been recently employed extensively to segregate diverse varieties of bio-particles such as CTCs [11], blood cells [23], parasites [24] and DNA [25]. A comprehensive study on the designs pertaining to applications of DLD technique along with their limitations was presented in [48]. A contorted arrangement of array of microposts can affect the functioning of DLD devices. Researchers have tested the technique by changing the micropost geometric shapes from circularly sized to triangular, and by the observation of trajectory of microbeads, it was deduced that the critical size parameter reduced in such arrays, and so particles of smaller size could be isolated using a larger device [26]. For example, using this concept, CTCs were captured from the blood sample flow with a segregation efficiency greater than 85% by involving triangular posts [27]. I-shaped pillars were used to separate RBCs and Escherichia coli bacteria from blood samples by these arrays [28]. Other micropillar shapes, including L-shape, I-shape, inverted L-shape, inverted anvil shape, anvil shape and T-shape have also been tried to segregate microbeads and RBCs [29]. In order to introduce asymmetry, the ratio between lateral gap and downstream gap was successfully tuned in DLD arrays to obtain suitable critical particle diameter using which RBCs were isolated with improved resolution [30]. A pseudoperiodicity model was also studied by observing the nanobead trajectories based on varying the downstream microposts gap to the lateral microposts gap ratio. From the measurement of migration angle of particles, it was found that the particles do not necessarily deflect to their angle of maxima because of the distinction between the flow pattern and the symmetry of posts [31]. Tracing of microbeads path patterns for various DLD arrays through experiments was conducted to observe particle behaviors in devices where anisotropy is introduced by array. Asymmetry was enhanced by varying the aspect ratio of arrays, i.e., horizontal posts gap to vertical posts gap ratio and modifying the shapes of microposts [32]. Fabrication of a sieve shape-based DLD style device was also done using asymmetry where three distinctly sized particles have been used for finding out the critical particle size [33]. Computational simulation study of modeled DLD-based devices can provide a clear picture for better assessment of the trajectories taken by particles. Different micropost shapes such as airfoil [34], triangle [27], I [28] and optimized shaped [35] post shapes have extensively been

considered for study apart from circular posts [36]. Lattice Boltzmann method was also used for computing the flow lane width in a DLD-based device considering variable lateral post gap size to downstream posts gap size ratios [37]. Asymmetry in such devices was further analyzed by computing the ratio of fluid flow lanes, though the mixed motion behavior of particles observed by experiments could not be explained and estimated [38]. For simulation of the behavioral pattern of firm and deformable particles, a coarse-grained mesoscopic method was used in a DLD device with a variety of micropillar shapes, including circular, diamond, square and triangular microposts [39]. A heuristic formula representing the critical particle diameter was estimated for cases in DLD where the horizontal post spacing and vertical post spacing are not equal [40]. Recently a 3D framework employing a lattice of representative resistors has been proposed to provide an advanced approach for analyzing periodic boundary conditions in DLD arrays [41]. Using the finite element method (FEM) simulation, an attempt to further alter the critical diameter equation was made. However, the revised critical diameter expression lacked accuracy for few of the experimental cases [30]. While simulating the working of a DLD device model, the influence of particle trajectory on the fluid flow profile and vice versa have to be carefully considered. Thus, it becomes a very challenging task to precisely present a visual representation of pathways of particles in a numerical-based simulation [42], but using computational analysis, we can get better insight of the device design and provide in-depth estimation of the device behavior before commencing the fabrication process.

Even though various studies have been conducted on the geometrical arrangement of the DLD array, but a definite thorough study on the effect of angle of release of bio-particles on their trajectory through DLD array is not available so far. In this simulation study, complete trajectory analysis of CTCs and WBCs has been performed using COMSOL Multiphysics software with respect to the angular orientation of sample inlet channel. Further for an efficient design of microfluidic device, apart from purity of extracted cells, it is also necessary to ensure that the trapped cells at outlets do not lose cellular structural property. In this paper, model of an asymmetric DLD array-based microfluidic device has been presented with optimized sample inlet orientation so as to maintain perfect separation efficiency of CTCs along with arrangement for unruptured trapping of CTCs and WBCs. We have used the latest empirical expression for critical diameter to make the simulated design of DLD array incorporate the experimental findings so far in this area. The obtained results show that the modeled device works fine at a much high value of sample mass flow rate for clear CTC–WBC isolation with appreciable efficiency and maintains minimum CTC–WBC interaction reducing chances of cell rupture.

## 2 Theory of deterministic lateral displacement

The characterizing parameter for particle isolation in DLD devices happens to be the size of the particles; thus, estimation of the critical structural size for particle segregation in a DLD-based device becomes very vital. This principle of design based on determining the critical particle diameter in a DLD-based device with same downstream post gap and lateral post gap sizes has been exploited [11]. As per this design logic, every spacing between two consecutive microposts in a particular row is split into fluidic lanes, termed as the array periodicity. Equal volumetric quantity of fluid is maintained by each of these flow lanes, and assuming a symmetrical parabolic flow profile, width of each lane can be estimated. On the basis of this theoretical arrangement, if the radius of the particle in the flow lane closest to the micropost is smaller in magnitude than the calculated width of lane, the particle traverses the path following that lane. This pattern of movement is coined as the "zigzag" mode. Otherwise, if the radius of particle exceeds the calculated width of lane, the particle deviates to the adjoining flow lane. This pattern of particle travel is termed as the "displacement" mode, also referred to as "bump" mode. Adoption of the pathway for any particle released in a fluid sample injected in a DLD array is dependent on the critical diameter ($D_c$). As presented in Fig. 1, particles with effective diameter lesser than $D_c$ follow a zigzag scheme of traversal while those with diameter larger than $D_c$ showcase a bumped pattern of traversal around the microposts [30]. In a DLD-based microfluidic device, the row shift fraction ($\varepsilon$) stands for a geometry-based parameter defining the ratio of displaced gap between the microposts and center-to-center distance of adjoining microposts. A quantifying parameter to indicate lateral row shifting of microposts in DLD array is termed tilted angle ($\theta$) representing the slope of micropost arrays. A period number ($P_N$) is defined for the array which means that the microposts of row $P_N + 1$ placed at the same slanting position as the primitive row.

## 3 Microfluidic device design and analysis

### 3.1 Layout of the proposed model of microfluidic device

Making use of COMSOL Multiphysics 5.4 software, a 3D layout view of the simulated model of microfluidic device centrally supported by the arrangement of asymmetric DLD array of cylindrical microposts has been designed. As presented in Fig. 2, at injecting end, three evenly positioned inlets namely two diagonal inlets for buffer fluid (water)
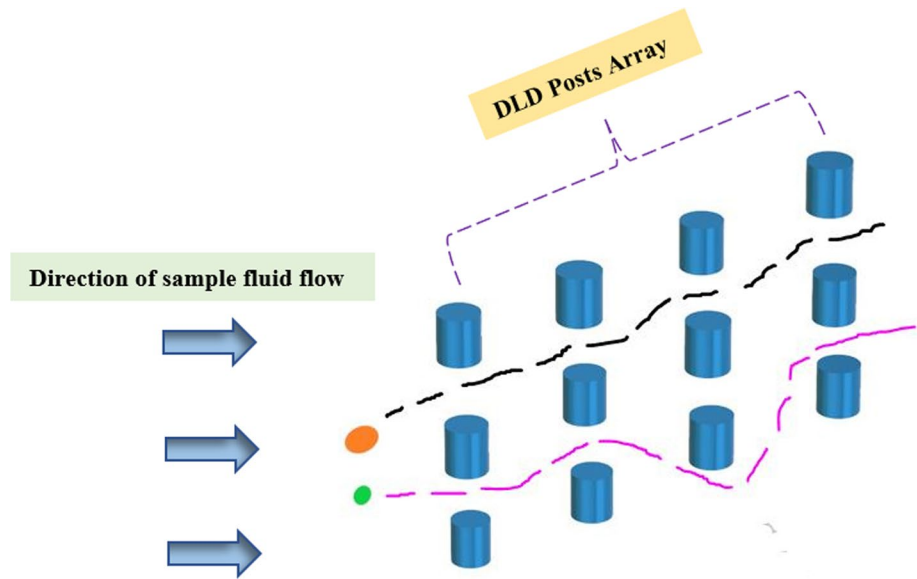
and one central inlet for sample (blood) have been built. Uniformly spaced multiple outlets have been provided for suitable extraction of distinct CTCs and WBCs and also to maintain steady and uniform pressure distribution within the device. The longitudinal spread of the device is 400 μm, and its width is fixed at 200 μm. The height of the cylindrical-shaped microposts is 30 μm.

## 3.2 Geometrical details of asymmetric DLD array for simulation study

Figure 3 puts on display the various dimensional parameters involved in selecting the design of asymmetric DLD array.

Table 1 lists out the various values of the characterizing asymmetric DLD array parameters placed within the microfluidic device.

Additionally, the lateral post gap to the perpendicular post gap size ratio between microposts can be expressed as:
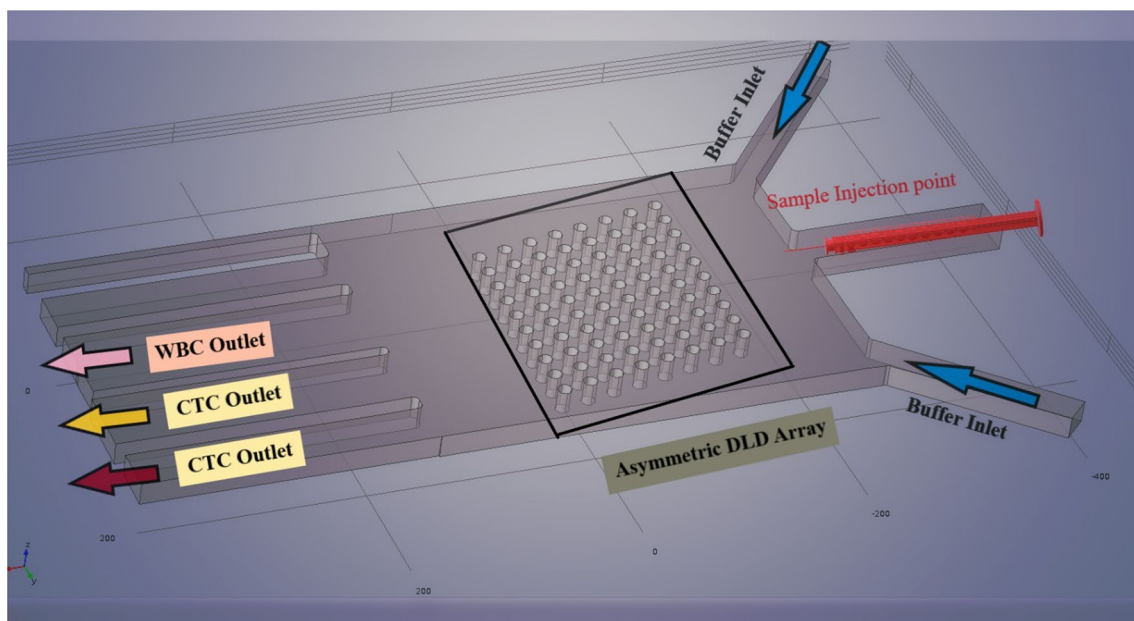


Fig. 2 3D view of the modeled microfluidic device

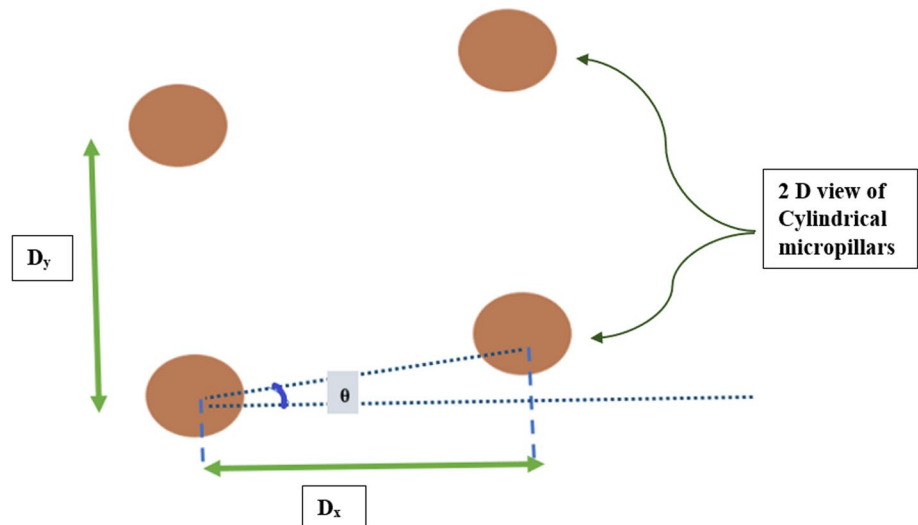**Fig. 3** Distinct geometrical design parameters for asymmetric DLD array



**Table 1** Values of distinct DLD array parameters

| Parameter | Parameter meaning | Parameter value chosen |
|---|---|---|
| $D_m$ | Diameter of microposts | 12 μm |
| $D_y$ | Perpendicular gap size between microposts | 21 μm |
| $D_x$ | Lateral gap size between microposts | 25 μm |
| $\tan(\theta)$ | Slope of micropost array | 0.199 |

$$\delta = \frac{D_x}{D_y} \tag{1}$$

The values of $\delta$ can be adjusted to bring in the effect of asymmetry in the cell trajectory inside the microfluidic device.

### 3.3 Governing equations for cell trajectory study

In the miniaturized mode, the fluid flow profile within the microfluidic device resembles the pattern observed in creeping regime, so simplification of Navier–Stokes equation is possible when the inertial force terms are neglected [43]. Hence, for the fluid stream in microfluidic device, the following equation can be implemented to govern the simulation [44]:

$$\rho_f \frac{\partial v_f}{\partial t} = -\nabla p_f + \eta \nabla^2 v_f \tag{2}$$

where $\rho_f$, $v_f$, $p_f$ and $\eta$ refer to density of fluid, velocity of fluid, pressure exerted by fluid and dynamic viscosity of fluid, respectively.

For tracing out the cell movement through the microfluidic device, Newton's second law is used, according to which the total force exerted on the cell equals the time rate of change of its linear momentum [45]:

$$\frac{d(m_c v_c)}{dt} = F_{bc} \tag{3}$$

where $m_c$, $v_c$ and $F_{bc}$ denote the cell mass, cell velocity and the total body force exerted on the cell, respectively. In our cell trajectory simulations, the drag force has been considered the single force exerted to the cell because of viscosity of fluid and the pressure gradient.

### 3.4 Theoretical analysis for evaluation of critical diameter ($D_c$)

As per the existing widely accepted generalized empirical model of DLD, the critical size of separation can be represented as [46]:

$$D_c = 1.4.g.\varepsilon^{0.48} \tag{4}$$

A more generalized expression of critical diameter has been deduced after several experimentation with introducing different levels of asymmetry in DLD array which can be represented as [47]:

$$\frac{D_c}{D_y} = 2.44\left(\frac{\epsilon}{\delta}\right)^{0.17} - 1.096\delta^{-0.558} \tag{5}$$

where the row shift fraction can be presented as [47]:

$$\varepsilon = \frac{(D_x + D_m)\tan\theta}{D_y + D_m} \tag{6}$$

As per our internal geometrical arrangement, listed in Table 1, in asymmetric DLD array centered within the microfluidic device, the parameter values are $\varepsilon = 0.224$, $\delta = 1.190$. Now, using Eq. (5), the critical diameter for the microfluidic device comes out to be:

$$\frac{D_c}{D_y} = 2.44\left(\frac{0.224}{1.190}\right)^{0.17} - 1.096(1.190)^{-0.558}$$

Thus $D_c = 212.44(0.7528) - 1.096(0.9074) = 17.688\mu m$.

In accordance with the particle movement pattern in DLD arrays, it can be established that for the proposed DLD design, any bio-particle with diameter greater than 17.688 μm will follow bumped mode whereas the ones lesser in size than $D_c$ shall follow zigzag mode.

# 4 Result and discussion

In this section, we have presented the simulation responses which were obtained after computationally analyzing the microfluidic device in COMSOL Multiphysics 5.4 software. In our simulation study, the microposts have been assumed to be rigid bodies, and the cells have been modeled as circular microbeads with physical properties same as actual cell characteristics. The characteristics of blood at room temperature have been used to model the sample fluid flow environment. In order to nullify the extra sidewall collision impacts on the cell trajectories, the microbeads are allowed to initiate their travel at the middle section of the microfluidic device much far away from the walls. Authentic cell characteristic parameter values as referenced in [46] have been used for trajectory study as presented in Table 2. The effect of angle at which the blood sample is injected within the microfluidic device on cell trajectory has been closely observed and presented through particle tracing feature in computational software tool.

## 4.1 Simulation response showing the effect of variation in anticlockwise orientation of sample inlet channel

By making use of the particle tracing feature of COMSOL Multiphysics 5.4, the microfluidic device was tested by injection of a blood sample containing representative WBCs

**Table 2** Distinct bio-particle parameters used for cell travel tracing in microfluidic device

| Bio-particle type | Mass (pg) | Diameter (μm) |
| --- | --- | --- |
| Lung cancer CTC | 36.8 | 22.4 |
| WBC | 19.3 | 12 |

and lung cancer CTCs at sample inlet. As shown in Sect. 3.4, the value of $D_c$ for the modeled device is 17.688 μm. So, as per the principle of DLD, lung cancer CTCs are expected to follow the displaced mode whereas the WBCs shall abide by the zigzag pattern. The obtained responses are in accordance with the theoretical estimation. Figure 4a–f shows the different movement patterns which the CTCs and WBCs trace out as the angle of injection changes in anticlockwise sense at the sample mass flow rate of $22 \times 10^{-6}$ kg/s. The mass flow rates of upward buffer inlet (water) and downward buffer inlet (water) were maintained at $40 \times 10^{-6}$ kg/s and $45 \times 10^{-6}$ kg/s, respectively.

Figure 4a shows a distinct separation of lung cancer CTCs from WBCs when the injection inlet is maintained exactly in same line with the horizontal axis crossing the midline of the asymmetric DLD array.

As we increase the tilt of injection inlet slowly in steps of 0.2° in anticlockwise sense, i.e., the release end facing toward the upper section of the DLD array, we notice that the device continues to isolate the CTCs effectively until the orientation is at 0.4°.

From 0.5° onward, as we provide angular displacement of injection inlet further, we observe that the distinctness of CTC–WBC separation shows a declining trend.
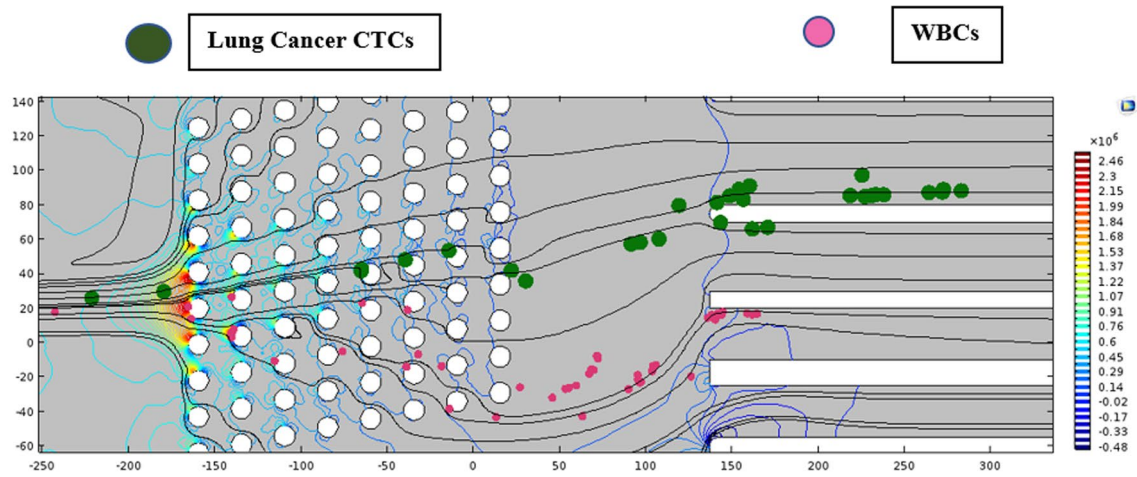
At 0.6° orientation, intermingling of CTCs and WBCs can be observed in the trajectory visualization indicating significant CTC–WBC collisions as the blood sample enters the DLD array.

The same trend of significant interaction between the cells at the passage of DLD array microposts continues as we increase the tilt further as can be seen with orientation at 0.8° in Fig. 4f.

## 4.2 Simulation response showing the effect of variation in clockwise orientation of sample inlet channel

By making use of the particle tracing feature of COMSOL Multiphysics 5.4, the microfluidic device was tested by injection of a blood sample containing representative WBCs and lung cancer CTCs at sample inlet. Figure 5a–f shows the different movement patterns which the CTCs and WBCs trace out as the angle of injection changes in clockwise sense at the sample mass flow rate of $22 \times 10^{-6}$ kg/s. The mass flow rates of upward buffer inlet (water) and downward buffer inlet (water) were maintained at $40 \times 10^{-6}$ kg/s and $45 \times 10^{-6}$ kg/s, respectively.
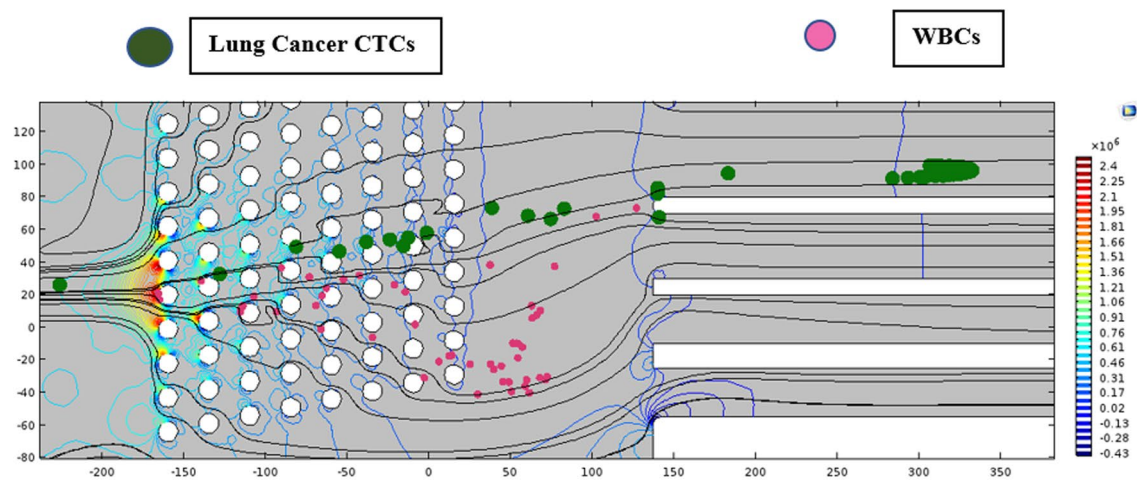
When the sample inlet is angularly displaced clockwise, i.e., the release end now facing the lower section of the DLD array, we observe that the isolation of CTCs from WBCs happens with a better distinctness when compared with the anticlockwise orientation.

**(a)** Simulation response for sample injection angle at $0^0$
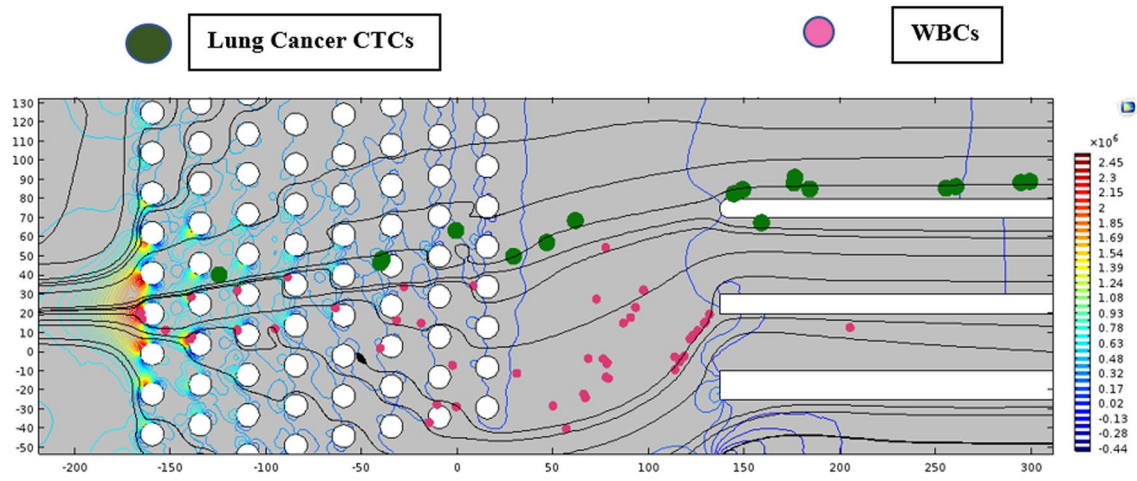


**(b)** Simulation response for sample injection angle at $0.2^0$



**(c)** Simulation response for sample injection angle at $0.4^0$

**Fig. 4** **a** Simulation response for sample injection angle at 0°. **b** Simulation response for sample injection angle at 0.2°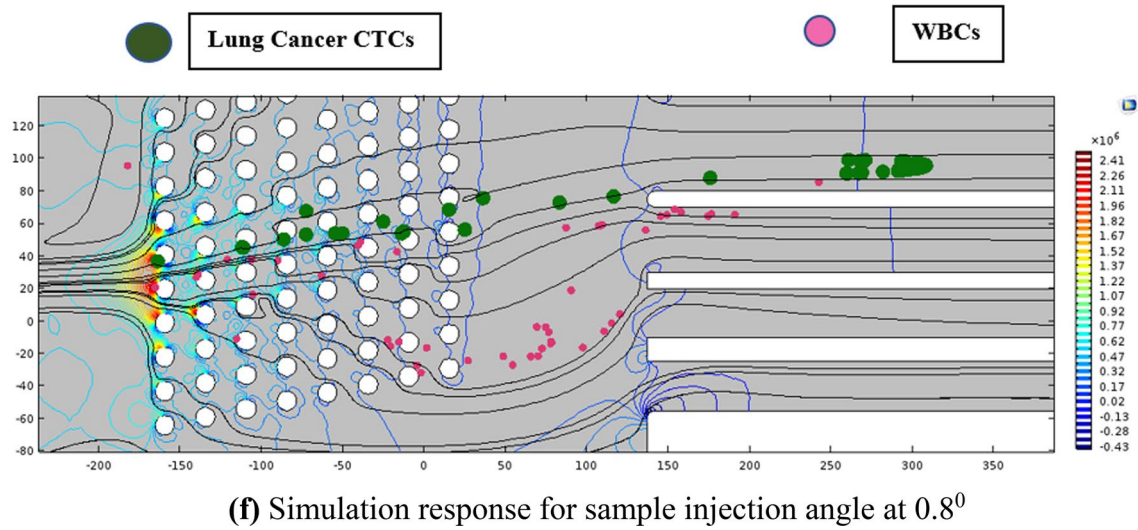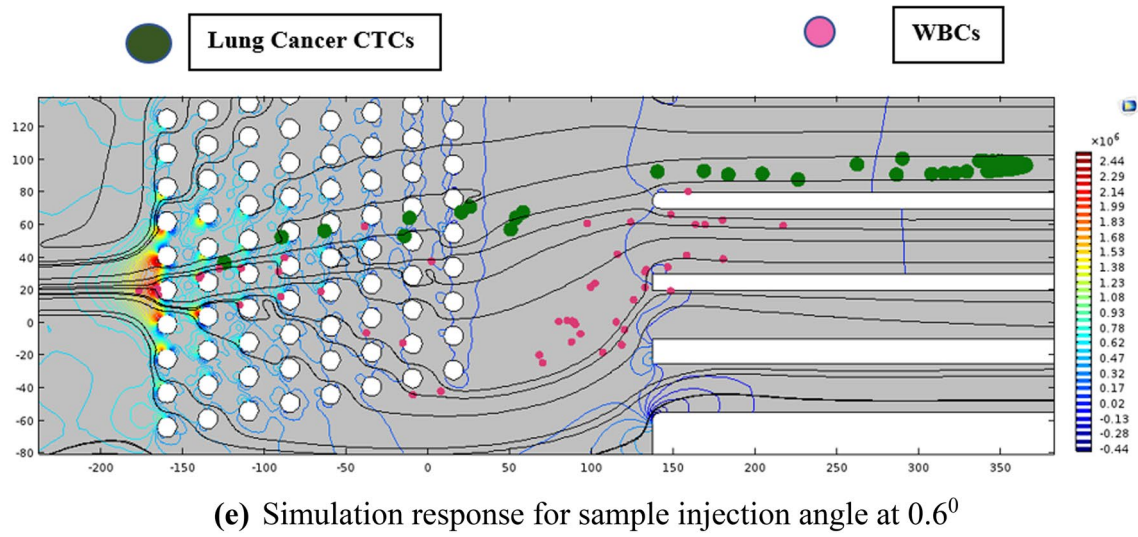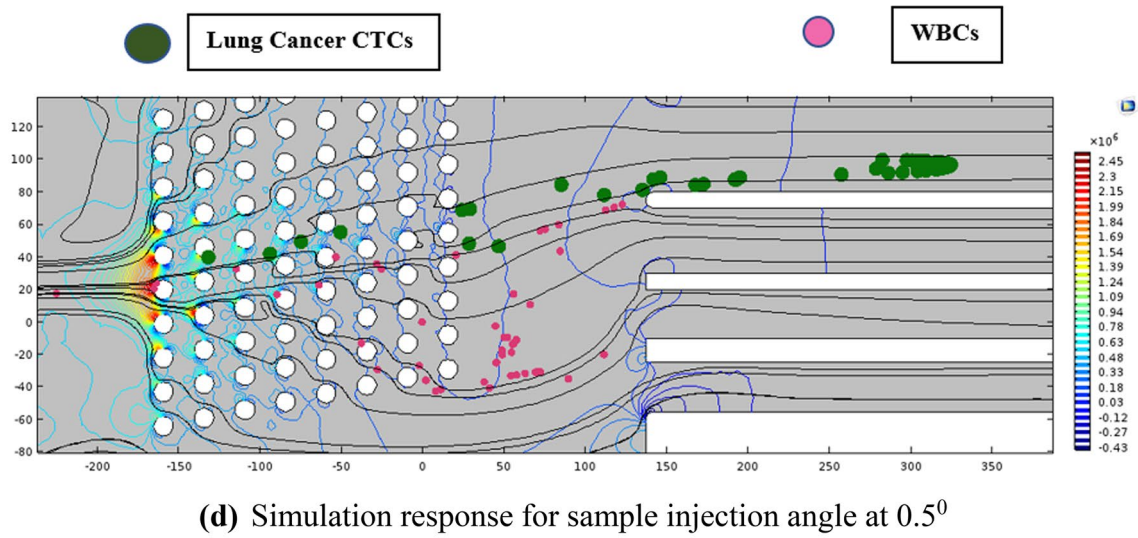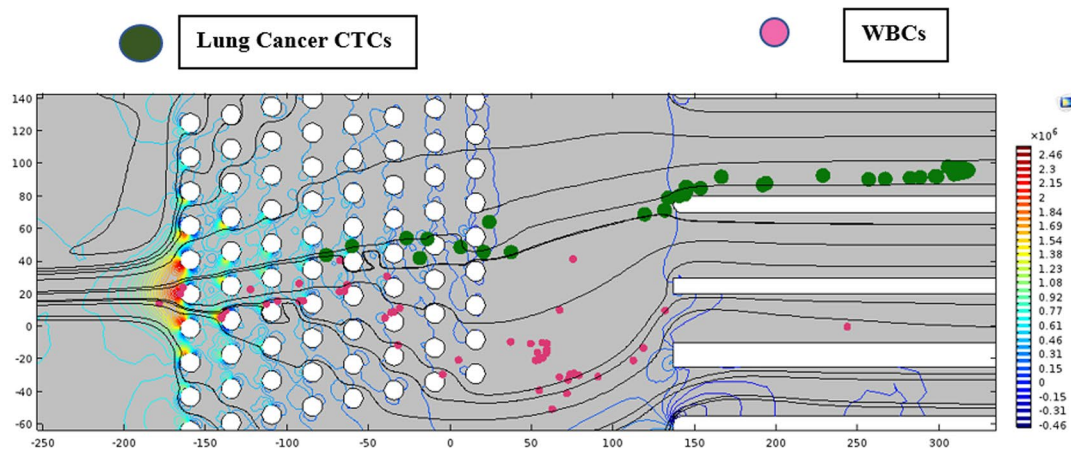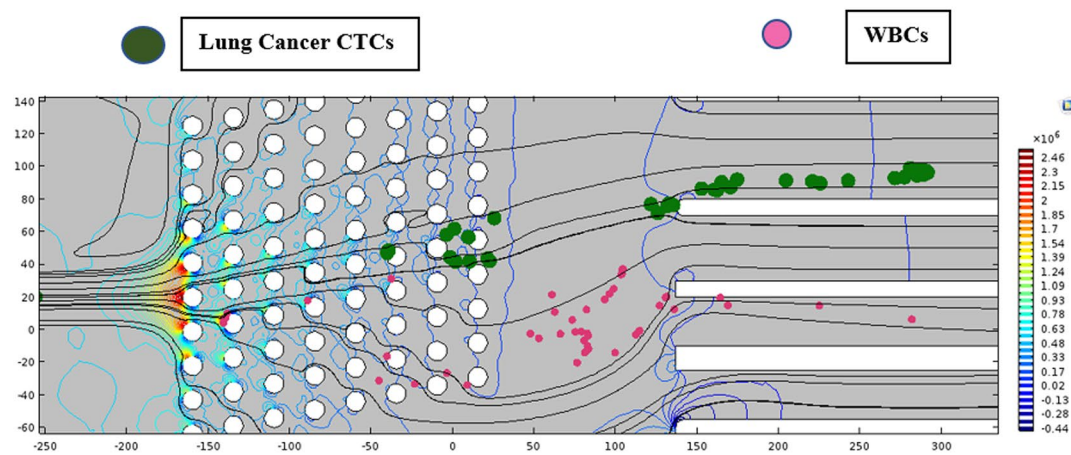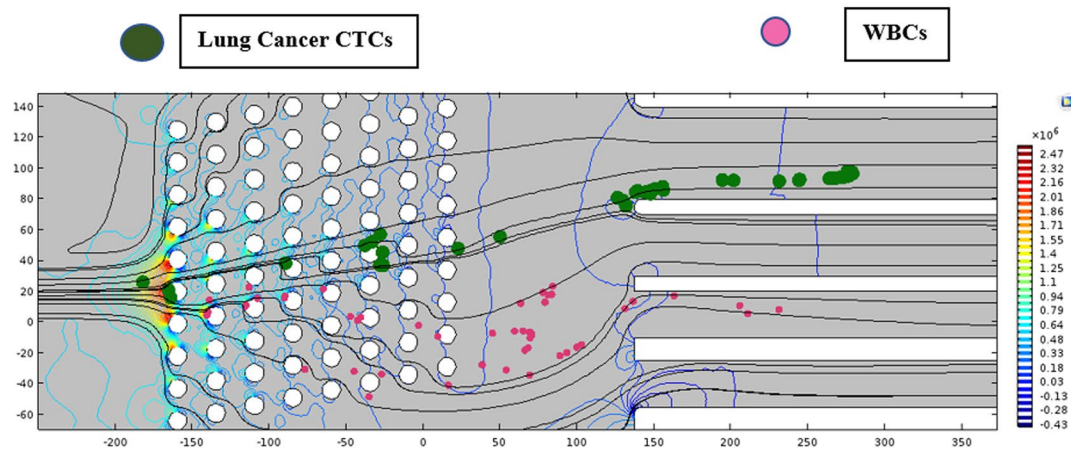. **c** Simulation response for sample injection angle at 0.4°. **d** Simulation response for sample injection angle at 0.5°. **e** Simulation response for sample injection angle at 0.6°. **f** Simulation response for sample injection angle at 0.8°

**(d)** Simulation response for sample injection angle at $0.5^0$



**(e)** Simulation response for sample injection angle at $0.6^0$



**(f)** Simulation response for sample injection angle at $0.8^0$

**Fig. 4** (continued)

**(a)** Simulation response for sample injection angle at $-0.1^0$



**(b)** Simulation response for sample injection angle at $-0.2^0$



**(c)** Simulation response for sample injection angle at $-0.4^0$

**Fig. 5** **a** Simulation response for sample injection angle at $-0.1°$. **b** Simulation response for sample injection angle at $-0.2°$. **c** Simulation response for sample injection angle at $-0.4°$. **d** Simulation response for sample injection angle at $-0.5°$. **e** Simulation response for sample injection angle at $-0.6°$. **f** Simulation response for sample injection angle at $-0.8°$

**(d)** Simulation response for sample injection angle at $- 0.5^0$



**(e)** Simulation response for sample injection angle at $- 0.6^0$



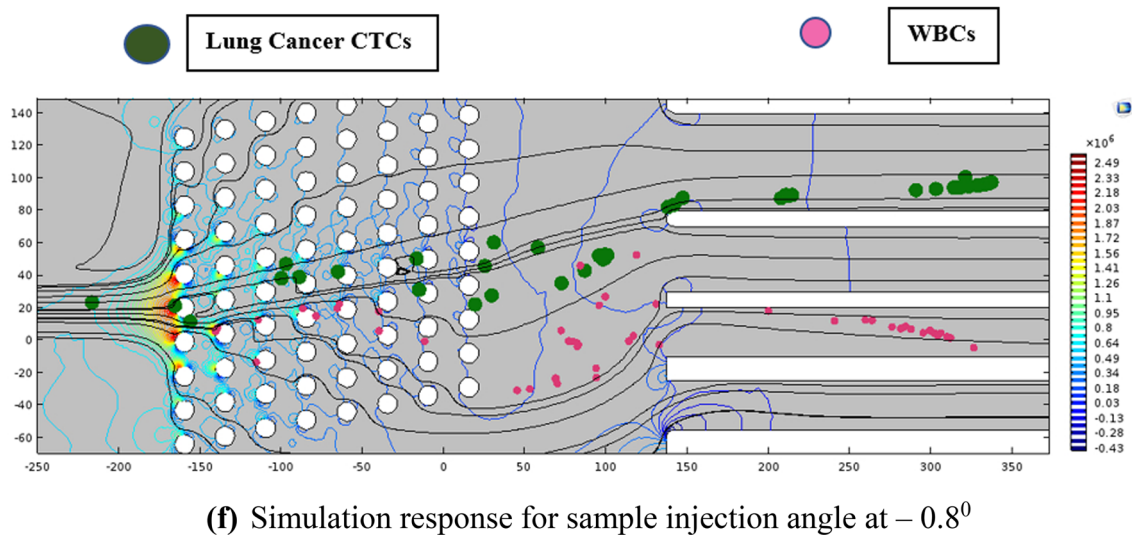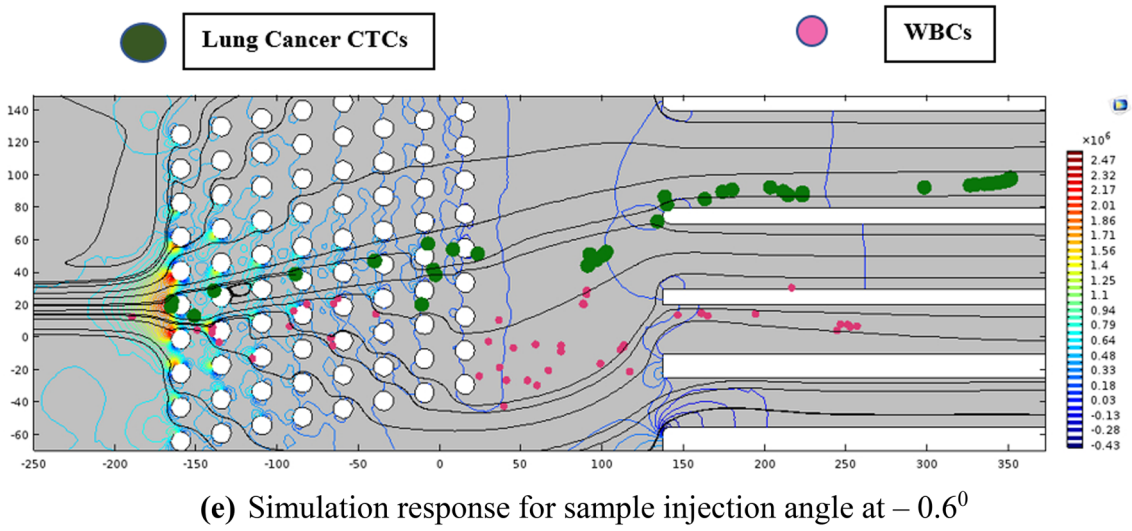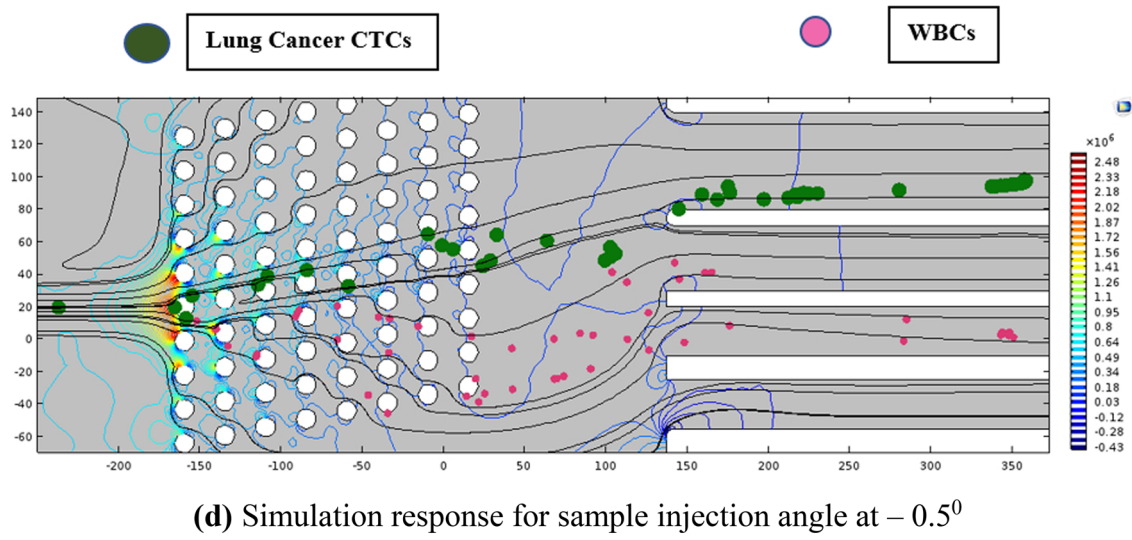**(f)** Simulation response for sample injection angle at $- 0.8^0$

**Fig. 5** (continued)

The distinct isolation pattern of CTCs continues as we increase the clockwise tilt of sample inlet channel toward 0.4° and 0.5°. It can be clearly observed from the responses shown in Fig. 5a–d that the displaced vertical gap between the trajectory patterns of CTCs and WBCs is wider enough when compared with the responses for anticlockwise tilt shown in Fig. 4a–d.

As shown in Fig. 5d, path tracing patterns of the two cells remain distinct with almost negligible interaction between them until the sample inlet tilt angle at − 0.5° as they enter the DLD array.

When the clockwise sample inlet tilt is increased beyond 0.5°, the distinctness of CTCs isolation still remains intact but some intermingling points of the CTCs and WBCs begin to emerge as shown in Fig. 5e, f.

At tilt of − 0.8°, a greater number of CTC–WBC interaction points can be noticed as shown in Fig. 5f, but the separation pattern is much better compared to the anticlockwise tilt of inlet channel.

### 4.3 Comparative study of CTC–WBC collision points for clockwise and anticlockwise orientation of sample injection inlet

In this section, we discuss the number of instances of CTC–WBC interaction within the microfluidic device as observed in the simulation response with variation in sample inlet orientation keeping the sample mass flow rate of $22 \times 10^{-6}$ kg/s constant. Figure 6a showcases the interaction area inside the DLD array for 0.9° anticlockwise sample inlet tilt which is the maximum permissible tilt for satisfactory CTC separation. It can be observed that there any interaction points indicating more possibility of cell rupture for both CTCs and WBCs.
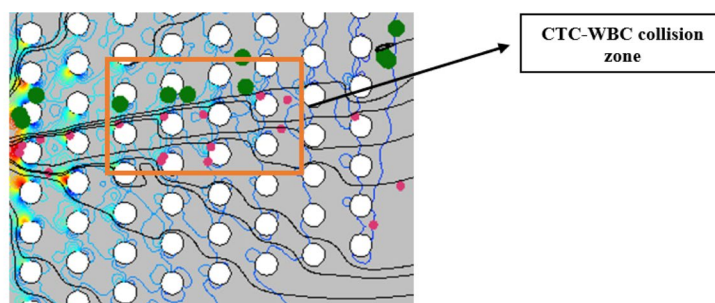
Figure 6b showcases the interaction area inside the DLD array for 0.9° clockwise sample inlet tilt. It can be observed that there are very few interaction points indicating negligible possibility of cell rupture for both CTCs and WBCs as per the simulation response obtained.

Figure 7 presents the plot showing the drastic difference in the number of instances CTCs and WBCs showed collision effect during their travel through DLD array under clockwise and anticlockwise sample inlet orientation effects. It can clearly be concluded that the usage of clockwise tilt in sample injection inlet reduces the risk of rupture of CTCs and WBCs making the device suitable for unruptured trapping at targeted outlets.
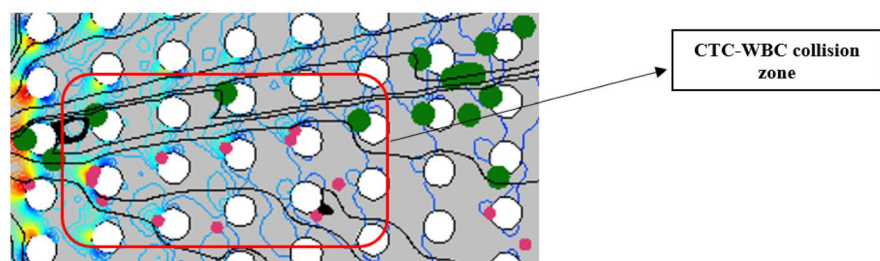
### 4.4 Comparative study of migration angle of CTC trajectory for clockwise and anticlockwise orientation of sample injection inlet

Migration angle can be expressed as a quantifying angular parameter to represent the maximum vertical lift that the CTCs take while following the bumped mode of travel within the asymmetrical DLD array. It can be defined as

**Fig. 6** **a** Zoomed image of cell trajectory showing CTC(Green marked)–WBC(Pink marked) interaction points for 0.9° anticlockwise sample inlet orientation. **b** Zoomed image of cell trajectory showing CTC(Green marked)–WBC(Pink marked) interaction points for 0.9° clockwise sample inlet orientation



**(a)** Zoomed image of cell trajectory showing CTC(Green marked)-WBC(Pink marked) interaction points for $0.9^0$ anticlockwise sample inlet orientation



**(b)** Zoomed image of cell trajectory showing CTC(Green marked)-WBC(Pink marked) interaction points for $0.9^0$ clockwise sample inlet orientation
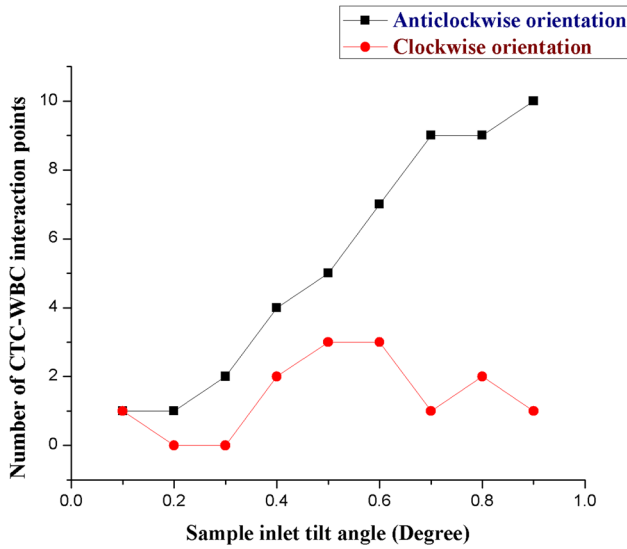
**Fig. 7** Plot showing variation in number of CTC–WBC interaction points with clockwise and anticlockwise orientation of sample inlet



**Fig. 8** Plot of maximum migration angle of CTC trajectory with variation in clockwise and anticlockwise orientation of sample inlet

$\theta_{\mathrm{mig}} = \tan^{-1}\left(\frac{y_{\mathrm{final}} - y_{\mathrm{initial}}}{x_{\mathrm{final}} - x_{\mathrm{initial}}}\right)$ where $(x_{\mathrm{initial}}, y_{\mathrm{initial}})$ represents the coordinate point of release of bio-particles (i.e., CTCs and WBCs) and $(x_{\mathrm{final}}, y_{\mathrm{final}})$ represents the ultimate coordinate point of the CTC showing the maximum vertical lift while traversing through the DLD array. It can prove to be a vital parameter to distinctly differentiate the two modes of bio-particle movement so that the CTCs and WBCs maintain a proper distance in terms of pathway to minimize the interaction between them. This will significantly reduce the chances of rupture of CTCs and WBCs. Figure 8 shows the plot of variation in migration angle for CTC trajectory as the sample inlet orientation is changed. It can be observed that for the different orientations, on an average the microfluidic device model offers $\theta_{\mathrm{mig}} \sim 15°$ for smooth isolation of CTCs without any significant cell rupture. The comparative analysis also reveals that anticlockwise tilting of sample inlet channel leads to a better migration angle for CTC trajectory.

### 4.5 Comparative study of separation efficiency of CTCs and WBCs for clockwise and anticlockwise orientation of sample injection inlet

Figure 9a presents the approximate cell separation efficiency figures as observed from the simulation responses with the anticlockwise tilting effect in sample inlet channel. It was observed that the CTC isolation efficiency remains above 95% until the inlet orientation is at 0.5°. Further tilting causes decrement in CTC isolation efficiency. A similar pattern of decrement in WBC separation efficiency as well. Thus, it can be deduced that in the anticlockwise sense,
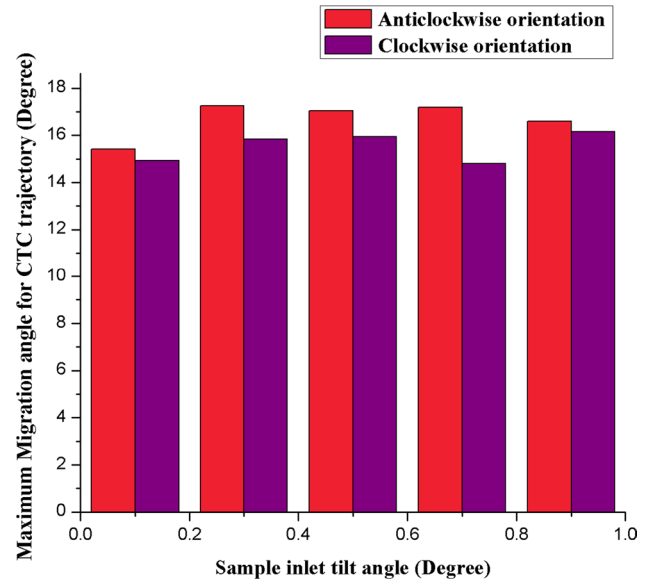
maximum tilt needs to be restricted to 0.5° for suitable CTC and WBC trapping at outlets.

Figure 9b presents the approximate cell separation efficiency figures as observed from the simulation responses with the clockwise tilting effect in sample inlet channel. It was observed that the CTC isolation efficiency remains above 95% until the inlet orientation is at 0.7°. Further tilting leads to dip in CTC isolation efficiency. A similar pattern of decrement in WBC separation efficiency as well. When compared with anticlockwise sample inlet tilt, the clockwise orientation generates better CTC and WBC isolation for a wider range. Thus, it can be deduced that in the clockwise sense, maximum tilt needs to be restricted to 0.7° for suitable CTC and WBC trapping at outlets.

### 4.6 Comparative study of shear rate around central microposts for clockwise and anticlockwise orientation of sample injection inlet

Shear rate is an important fluid parameter signifying the effect of viscosity of fluidic layers as the cells travel through the designated fluidic streamline. If the shear stress induced due to the sample flow rate through the inlet is maintained constant, then the shear rate is inversely proportional to viscosity. A higher value of shear rate would indicate lower viscosity and thus lesser resistance to the designated streamline for the CTC trajectory. In this section, the shear rate around the central microposts of the DLD array has been studied with respect to the variation in sample inlet orientation. The areas around those cylindrical microposts have been selected for the shear rate value through the CTCs are most likely to

**Fig. 9** **a** Plot of cell separation efficiency at designated outlet with variation in anticlockwise orientation in sample inlet channel. **b** Plot of cell separation efficiency at designated outlet with variation in clockwise orientation in sample inlet channel
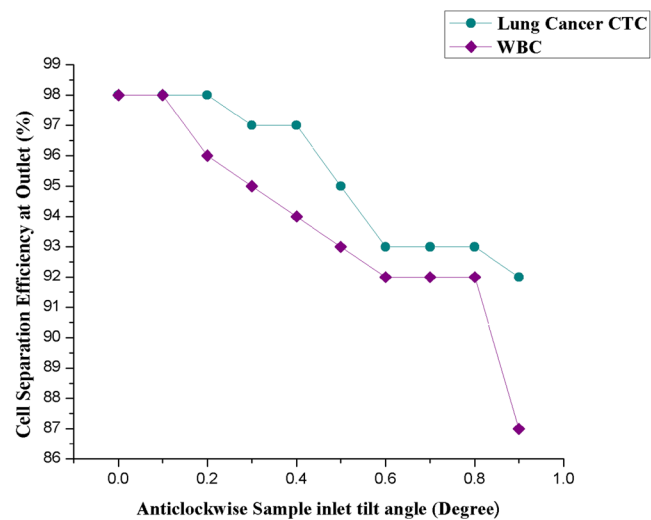


**(a)** Plot of cell separation efficiency at designated outlet with variation in anticlockwise orientation in sample inlet channel
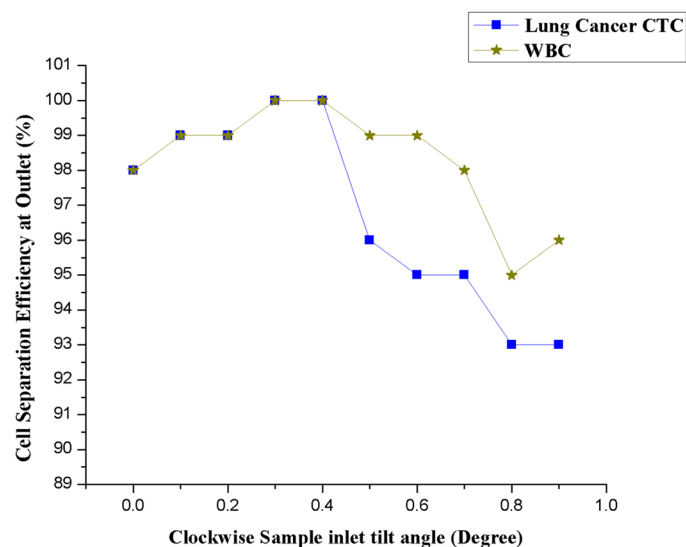


**(b)** Plot of cell separation efficiency at designated outlet with variation in clockwise orientation in sample inlet channel

traverse as per bumped mode of trajectory. Figure 10a shows the plot of shear rate around central microposts with the variation in anticlockwise sample inlet tilt. It can be observed that the shear rate is on the higher side until 0.5° orientation and any further inclination leads to downward trend in the shear rate figure.

Figure 10b shows the plot of shear rate around central microposts with the variation in clockwise sample inlet tilt. In this pattern of inlet orientation, the values of shear rate obtained were much higher than the anticlockwise orientation. This indicates that the CTC trajectory is expected to be much smoother with minimum restriction due to viscous force. It can also be observed that the shear rate is on the

higher side until 0.6° orientation and any further inclination leads to downward trend in the shear rate figure.

## 4.7 Numerical solution verification analysis of simulation results

In order to ascertain the validity of the obtained simulated results, we have run a grid/mesh convergence analysis of all the cell trajectory cases with different sample inlet inclinations. For an instance, we present the cell trajectory case with 0.5 degree clockwise orientation of sample inlet. With normal mesh, the cell trajectory response is shown in

**Fig. 10 a** Plot of shear rate (1/s) around central microposts with variation in anticlockwise orientation in sample inlet channel. **b** Plot of shear rate (1/s) around central microposts with variation in clockwise orientation in sample inlet channel
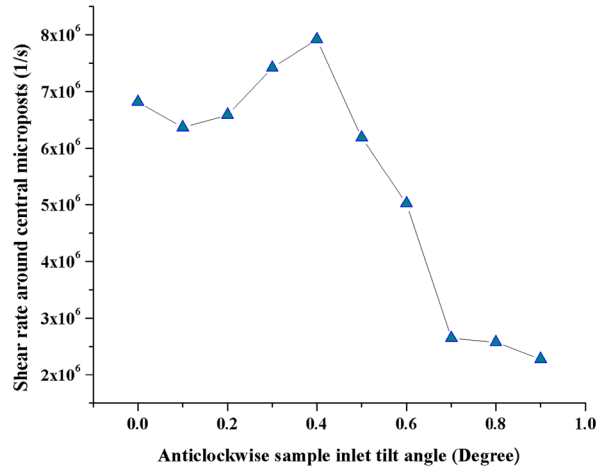


**(a)** Plot of shear rate (1/s) around central microposts with variation in anticlockwise orientation in sample inlet channel
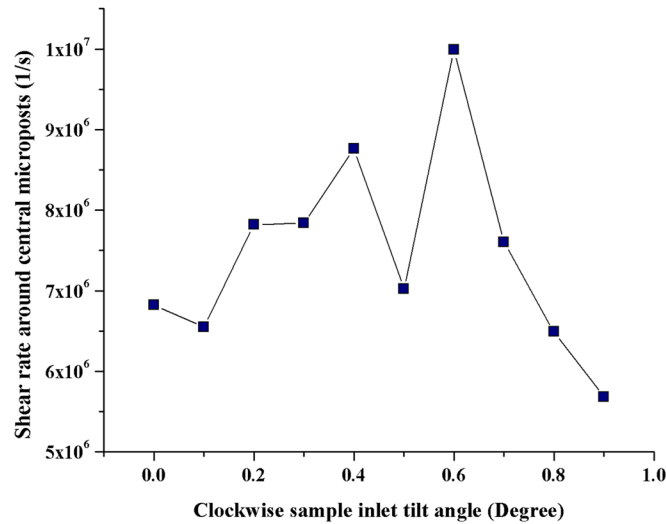


**(b)** Plot of shear rate (1/s) around central microposts with variation in clockwise orientation in sample inlet channel

Fig. 11a and the corresponding convergence plot as obtained from COMSOL Multiphysics software is shown in Fig. 11b.

To verify mesh independence, with fine mesh, the cell trajectory response is shown in Fig. 12a and the corresponding convergence plot as obtained from COMSOL Multiphysics software is shown in Fig. 12b.

Further, with finer mesh, the cell trajectory response is shown in Fig. 13a and the corresponding convergence plot as obtained from COMSOL Multiphysics software is shown in Fig. 13b.

From this analysis, it can be clearly observed that numerical solution convergence was obtained indicating valid cell trajectory patterns. Similar convergence plots were observed for all other simulation responses depicted in previous results. It can also be witnessed that even after altering the mesh arrangement, i.e., normal, fine and finer patterns, the cell trajectory points do not show alteration and hence meshing does not change cell separation efficiency.

## 5 Conclusion

We have successfully modeled an asymmetric DLD array-based microfluidic device using COMSOL Multiphysics 5.4 software for efficient lung cancer CTC–WBC isolation at a high sample mass flow rate of $22 \times 10^{-6}$ kg/s. In this simulation study, the effect of angle of release of cells from the sample inlet on the CTC–WBC trajectory through DLD array has been investigated. It was found that clockwise tilting of sample inlet channel yielded better results
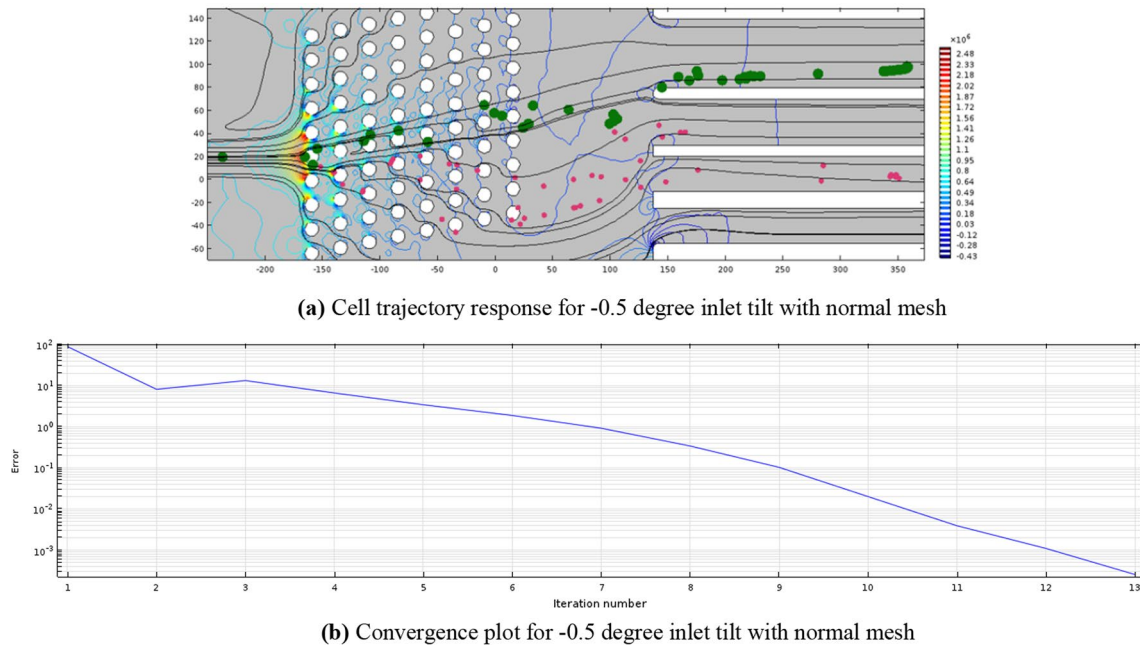
**(a)** Cell trajectory response for -0.5 degree inlet tilt with normal mesh



**(b)** Convergence plot for -0.5 degree inlet tilt with normal mesh

**Fig. 11** **a** Cell trajectory response for − 0.5 degree inlet tilt with normal mesh. **b** Convergence plot for − 0.5 degree inlet tilt with normal mesh



**(a)** Cell trajectory response for -0.5 degree inlet tilt with fine mesh



**(b)** Convergence plot for -0.5 degree inlet tilt with fine mesh

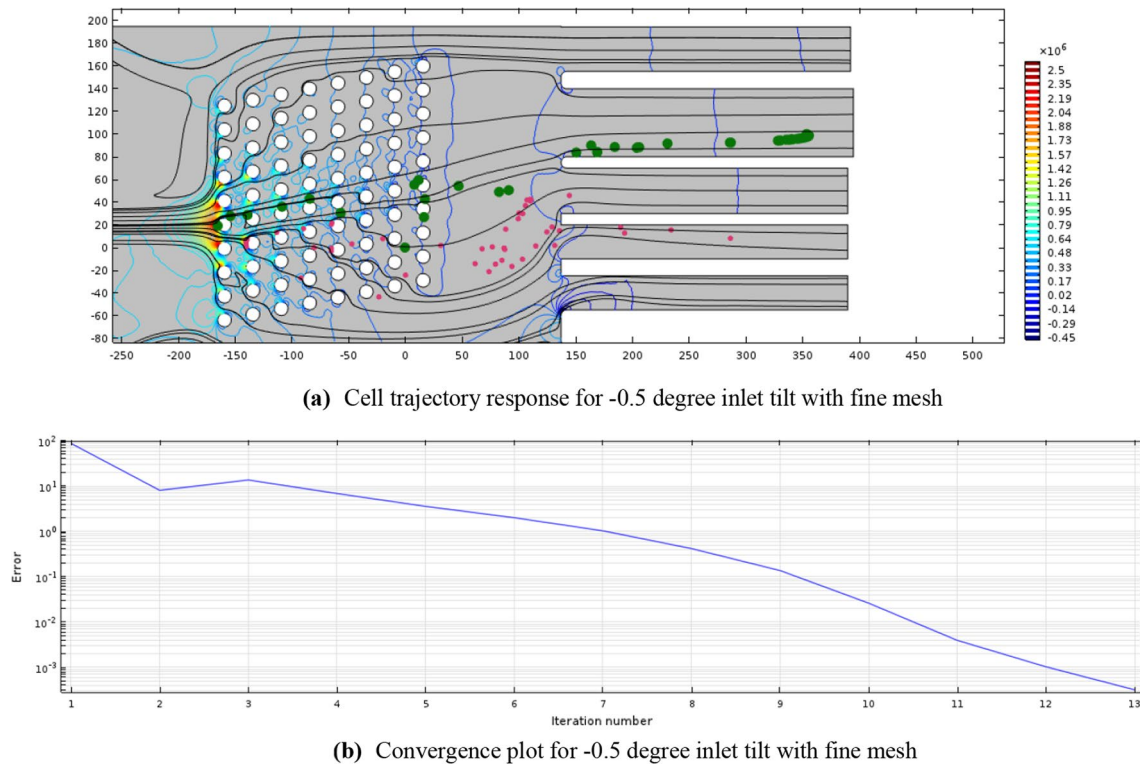**Fig. 12** **a** Cell trajectory response for − 0.5 degree inlet tilt with fine mesh. **b** Convergence plot for − 0.5 degree inlet tilt with fine mesh

compared to anticlockwise inclination. The approximate CTC isolation efficiency was obtained above 95% for sample inlet inclinations up to 0.5°, and further tilt showed reduction in efficiency. For clockwise sample inlet orientation, high isolation efficiency of cells was observed till 0.7°. Migration angle of CTC trajectory for the modeled
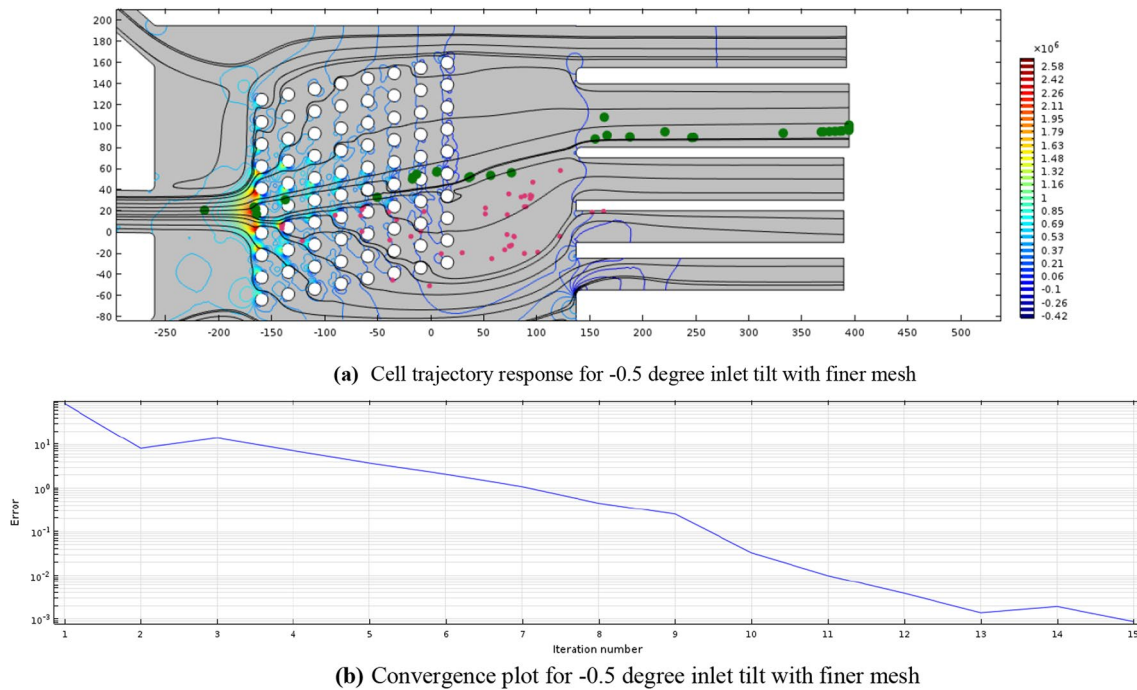
**(a)** Cell trajectory response for -0.5 degree inlet tilt with finer mesh



**(b)** Convergence plot for -0.5 degree inlet tilt with finer mesh

**Fig. 13** **a** Cell trajectory response for − 0.5 degree inlet tilt with finer mesh. **b** Convergence plot for − 0.5 degree inlet tilt with finer mesh

device was obtained around 15° for both the sample inlet orientations indicating clear distinctive pathways for CTC and WBC movement. The simulation responses revealed a smaller number of CTC–WBC interaction points for clockwise sample inlet tilt compared to the anticlockwise displacement. This reduces possibilities of cell rupture while traversing through the DLD array at high sample flow rate. The shear rate around central microposts was found to be higher in clockwise sample inlet orientation which leads to unrestricted travel of CTCs through the bumped mode. Thus, this study establishes that sample inlet clockwise tilting of maximum around 0.5°–0.7° leads to better CTC isolation and provides better chances of unruptured trapping of cells at the designated outlets. The results of this study provide an approach toward further optimization of DLD devices' functioning and, thus, could help fabricate better DLD-based microfluidic devices for efficient trapping of CTCs. Accurate modeling of the target cells such as CTCs can be done using equations in spherical domain for better tracking of movement of these cells inside the microfluidic device. This would help in improving preciseness of simulation results obtained by computational methods.

## Declarations

**Conflict of interest** The authors declare that they have no conflict of interest.

**Ethical approval** This article does not contain any studies with human participants or animals performed by any of the authors.

## References

1. Yin J, Deng J, Du C, Zhang W, Jiang X (2019) Microfluidics-based approaches for separation and analysis of circulating tumor cells. TrAC, Trends Anal Chem 117:84–100
2. Cortés-Hernández LE, Eslami-S Z, Alix-Panabières C (2020) Circulating tumor cell as the functional aspect of liquid biopsy to understand the metastatic cascade in solid cancer. Mol Aspects Med 72:100816

3.  Kozminsky M, Nagrath S, Liu H, Lathia J (2016) Circulating tumor cells, cancer stem cells, and emerging microfluidic detection technologies with clinical applications. In: Cancer stem cells, pp 473–497

4.  Li X, Li Y, Shao W, Li Z, Zhao R, Ye Z (2020) Strategies for enrichment of circulating tumor cells. Transl Cancer Res 9(3):2012

5.  Tang W, Jiang D, Li Z, Zhu L, Shi J, Yang J, Xiang N (2019) Recent advances in microfluidic cell sorting techniques based on both physical and biochemical principles. Electrophoresis 40(6):930–954

6.  Nasiri R, Shamloo A, Ahadian S, Amirifar L, Akbari J, Goudie MJ, Lee K, Ashammakhi N, Dokmeci MR, Di Carlo D (2020) Microfluidic-based approaches in targeted cell/particle separation based on physical properties: fundamentals and applications. Small 16(29):2000171

7.  Farahinia A, Zhang WJ, Badea I (2021) Novel microfluidic approaches to circulating tumor cell separation and sorting of blood cells: a review. J Sci: Adv Mater Dev 6(3):303–320

8.  Chang C-L, Huang W, Jalal SI, Chan B-D, Mahmood A, Shahda S, O'Neil BH, Matei DE, Savran CA (2015) Circulating tumor cell detection using a parallel flow micro-aperture chip system. Lab Chip 15:1677–1688

9.  Fan X, Jia C, Yang J, Li G, Mao H, Jin Q, Zhao J (2015) A microfluidic chip integrated with a high-density PDMS-based microfiltration membrane for rapid isolation and detection of circulating tumor cells. Biosens Bioelectron 71:380–386

10. Nathamgari SSP, Dong B, Zhou F, Kang W, Giraldo- Vela JP, McGuire T, McNaughton RL, Sun C, Kessler JA, Espinosa HD (2015) Isolating single cells in a neurosphere assay using inertial microfluidics. Lab Chip 15:4591–4597

11. Bhattacharjee R, Kumar R, Panwala FC, Shakeel PM (2020) Design and analysis of an optimized microfluidic channel for isolation of circulating tumor cells using deterministic lateral displacement technique. Complex Intell Syst 6(3):711–720

12. Chen Y, Wu M, Ren L, Liu J, Whitley PH, Wang L, Huang TJ (2016) High-throughput acoustic separation of platelets from whole blood. Lab Chip 16:3466–3472

13. Hajari M, Ebadi A, Farshchi Heydari MJ, Fathipour M, Soltani M (2020) Dielectrophoresis-based microfluidic platform to sort micro-particles in continuous flow. Microsyst Technol 26(3):751

14. Zhao Q, Yuan D, Zhang J, Li W (2020) A review of secondary flow in inertial microfluidics. Micromachines 11(5):461

15. Jigar Panchal H, Kent NJ, Knox AJ, Harris LF (2020) Microfluidics in haemostasis: a review. Molecules 25(4):833

16. Yager P et al (2006) Microfluidic diagnostic technologies for global public health. Nature 442:412–418

17. Shrimal P, Jadeja G, Patel S (2020) A review on novel methodologies for drug nanoparticle preparation: microfluidic approach. Chem Eng Res Des 153:728–756

18. Ashtari B et al (2020) Separating mouse malignant cell line (EL4) from neonate spermatogonial stem cells utilizing microfluidic device in vitro. Stem Cell Res Therapy 11(1):1–11

19. Gossett DR et al (2010) Label-free cell separation and sorting in microfluidic systems. Anal Bioanal Chem 397(8):3249–3267

20. Sajeesh P, Sen AK (2014) Particle separation and sorting in microfluidic devices: a review. Microfluid Nanofluid 17(1):1–52

21. Bayareh M (2020) An updated review on particle separation in passive microfluidic devices. Chem Eng Process Process Intensif 153:107984

22. Huang LR, Cox EC, Austin RH, Sturm JC (2004) Continuous particle separation through deterministic lateral displacement. Science 304(5673):987–990

23. Civin CI et al (2016) Automated leukocyte processing by microfluidic deterministic lateral displacement. Cytom Part A 89(12):1073–1083

24. Holm SH, Beech JP, Barrett MP, Tegenfeldt JO (2016) Simplifying microfluidic separation devices towards field-detection of blood parasites. Anal Methods 8(16):3291–3300

25. Wunsch BH et al (2019) Gel-on-a-chip: continuous, velocity-dependent DNA separation using nanoscale lateral displacement. Lab Chip 19(9):1567–1578

26. Loutherback K, Chou KS, Newman J, Puchalla J, Austin RH, Sturm JC (2010) Improved performance of deterministic lateral displacement arrays with triangular posts. Microfluid Nanofluid 9(6):1143–1149

27. Loutherback K, D'Silva J, Liu L, Wu A, Austin RH, Sturm JC (2012) Deterministic separation of cancer cells from blood at 10 mL/min. AIP Adv 2(4):042107

28. Zeming KK, Ranjan S, Zhang Y (2013) Rotational separation of non-spherical bioparticles using I-shaped pillar arrays in a microfluidic device. Nat Commun 4(1):1–8

29. Ranjan S, Zeming KK, Jureen R, Fisher D, Zhang Y (2014) DLD pillar shape design for efficient separation of spherical and non-spherical bioparticles. Lab Chip 14(21):4250–4262

30. Zeming KK, Salafi T, Chen C-H, Zhang Y (2016) Asymmetrical deterministic lateral displacement gaps for dual functions of enhanced separation and throughput of red blood cells. Scient Rep 6:22934

31. Kim S-C, Wunsch BH, Hu H, Smith JT, Austin RH, Stolovitzky G (2017) Broken flow symmetry explains the dynamics of small particles in deterministic lateral displacement arrays. Proc Natl Acad Sci 114(26):E5034–E5041

32. Vernekar R, Krüger T, Loutherback K, Morton K, Inglis DW (2017) Anisotropic permeability in deterministic lateral displacement arrays. Lab Chip 17(19):3318–3330

33. Dijkshoorn J, Schutyser M, Sebris M, Boom R, Wagterveld R (2017) Reducing the critical particle diameter in (highly) asymmetric sieve-based lateral displacement devices. Sci Rep 7(1):1–10

34. Ahasan K, Landry CM, Chen X et al (2020) Effect of angle-of-attacks on deterministic lateral displacement (DLD) with symmetric airfoil pillars. Biomed Microdevices 22:42

35. Hyun J-C, Hyun J, Wang S, Yang S (2017) Improved pillar shape for deterministic lateral displacement separation method to maintain separation efficiency over a long period of time. Separat Purif Technol 172:258–267

36. McGrath J, Jimenez M, Bridle H (2014) Deterministic lateral displacement for particle separation: a review. Lab Chip 14(21):4139–4158

37. Kulrattanarak T, Van Der Sman R, Schroën C, Boom R (2011) Analysis of mixed motion in deterministic ratchets via experiment and particle simulation. Microf Nanofluid 10(4):843–853

38. Kulrattanarak T et al (2011) Mixed motion in deterministic ratchets due to anisotropic permeability. J Colloid Interf Sci 354(1):7–14

39. Zhang Z, Henry E, Gompper G, Fedosov DA (2015) Behavior of rigid and deformable particles in deterministic lateral displacement devices with different post shapes. J Chem Phys 143(24):243145

40. Inglis D (2007) Microfluidic devices for cell separation. Princeton University

41. Inglis D, Vernekar R, Krüger T, Feng S (2020) The fluidic resistance of an array of obstacles and a method for improving boundaries in deterministic lateral displacement arrays. Microf Nanofluid 24(3):1–8

42. Hochstetter A et al (2020) Deterministic lateral displacement: challenges and perspectives. ACS Nano 14(9):10784–10795

43. Beebe DJ, Mensing GA, Walker GM (2002) Physics and applications of microfluidics in biology. Ann Rev Biomed Eng 4(1):261–286

44. Squires TM, Quake SR (2005) Microfluidics: fluid physics at the nanoliter scale. Rev Modern Phys 77(3):977

45. Das D, Biswas K, Das S (2014) A microfluidic device for continuous manipulation of biological cells using dielectrophoresis. Med Eng Phys 36(6):726–731

46. Bhattacharjee R, Kumar R, Al-Turjman F (2022) A novel approach for tuning of fluidic resistance in deterministic lateral displacement array for enhanced separation of circulating tumor cells. Cogn Comput 14:1660–1676. https://doi.org/10.1007/s12559-021-09904-y

47. Rezaei B, Zand MM, Javidi R (2021) Numerical simulation of critical particle size in asymmetrical deterministic lateral displacement. J Chromatogr A 1649:462216

48. Salafi T, Zhang Y, Zhang Y (2019) A review on deterministic lateral displacement for particle separation and detection. Nano-Micro Lett 11:77

**Publisher's Note** Springer Nature remains neutral with regard to jurisdictional claims in published maps and institutional affiliations.